ROYAL SOCIETY OF CHEMISTRY

PAPER

Check for updates

Efficient production of uniform gold nanoparticles *via* a streamlined low-cost, semi-automated, open-source platform

Suhash Reddy Chavva,[a,b] Angela Michelle T. San Juan, [a,b] Siddhant Jaitpal, [a,b] Ngoc Nhu Vu[a,b] and Samuel Mabbott [★a,b]

In the quest to discover dependable and repeatable methods for producing noble metal nanospheres, both commercial and academic scientists have shown great interest. The challenge of precisely controlling the size of these nanospheres is critical, as variations can alter their optical characteristics, leading to complications in subsequent applications. In this context, we present the design and validation of an affordable, semi-automated device that synthesizes gold nanoparticles using the Turkevich method. This device, named 'NanoSynth Mini' and powered by Raspberry Pi, demonstrates the capability to generate gold nanoparticles with diameters ranging from 15 to 60 nanometers with minimal variability. Its design allows for seamless integration into lab processes, providing consistent support for extensive research initiatives.

Introduction

Spherical gold nanoparticles (GNPs) have been applied to a wide variety of applications that span the breadth of biological and chemical sciences. Such applications include catalysis,[1–3] therapeutics,[4,5] antimicrobics,[6–8] and sensing.[9–11] Techniques for fabricating gold nanospheres can be broadly categorized into two approaches; top-down and bottom-up. Top-down methods employ techniques such as laser ablation[12,13] and nanolithography,[14] focusing on transforming bulk gold into smaller fragments. Many bottom-up approaches can be defined as chemical synthesis methods where metallic precursors and reducing agents are combined to form nanostructures. While lots of different combinations of metal salts and reducing agents of varying strengths exist, the most common way of synthesizing GNPs is *via* the Turkevich method, a single-phase process that was later refined by Frens.[15,16] Often referred to as citrate reduction, the Turkevich reaction involves the mixing and boiling of auric acid (HAuCl$_4$) with sodium citrate (Na$_3$C$_6$H$_5$O$_7$). By varying the ratiometric concentration of HAuCl$_4$: Na$_3$C$_6$H$_5$O$_7$ it is possible to create gold nanospheres with different diameters. Several alternative strategies for producing gold nanospheres with reproducible parameters exist, however, while alternatives exist very few are

as easy to replicate in comparison to the Turkevich method. One major advantage of the citrate reduction method is the amenability of the nanoparticles towards functionalization post-synthesis. The citrate acts as both a reducing and stabilizing reagent (capping agent), that is weakly, and electrostatically associated with the surface of the AuNPs. Overcoming the electrostatic association to perform surface functionalization with recognition elements or for the conjugation of surface modifiers is straightforward compared to when capping agents such as cetyltrimethylammonium bromide (CTAB), polyethylene glycol (PEG), chitosan, *etc*. are used to control the morphology and homogeneity of the particles.

While we can conclude that the Turkevich reaction is easy to perform and the resultant particles are more amenable to post-surface modifications, it is often difficult to maintain batch-to-batch nanoparticle consistency especially when nearly all current gold nanoparticle syntheses are performed manually.[17,18] Although a lot of research focuses on GNP synthesis and their applications, their use in everyday life is limited, as scale-up of conventional synthesis methods often suffers from reproducibility issues. The inability to sustain batch-to-batch nanoparticle reproducibility can severely hinder research progress, especially concerning the optimization of nanoparticle-integrated applications. Furthermore, the purchase of commercially available nanoparticles for developmental research can be cost-prohibitive and without the use of stabilizing reagents, there is no guarantee of how long the particles will remain dispersed.

ª Department of Biomedical Engineering, Texas A&M University, College Station, Texas, USA. E-mail: smabbott@tamu.edu
ᵇ Health Technologies and Innovations Center, Texas A&M University, College Station, Texas, USA

Over the past few years, a number of researchers have recognized the potential advantages of automated nanoparticle synthesis. However, many challenges remain in optimizing the automated synthesis of colloidal nanoparticles. Switching from manual to automated chemical processes has already been successfully demonstrated in polypeptide,[19] oligosaccharide,[20] and organic synthesis[21] to improve product yields whilst minimizing side products. Furthermore, several of these groups have implemented evolutionary and statistical algorithms to discover *de novo* synthesis pathways. However, very few groups have tried to automate the synthesis of GNPs. The most influential work to date was carried out by Cronin and co-coworkers, who used a Darwinian evolutionary algorithm to optimize reaction conditions to synthesize spherical, rod shaped, and octahedral GNPs on a closed loop robot platform in a controlled and reproducible manner.[22] Further, several researchers have performed the synthesis of GNPs in continuous flow microfluidic reactors,[23–27] due to the inherent advantages associated with the use of milli- and microreactors such as timing of reagent addition, control over mass and heat transfer, mixing conditions and reproducibility of the products and their properties. Although, microfluidic nanoparticle synthesis has its advantages, they have been shown to be highly prone to irreversible fouling (blockage) during nanoparticle synthesis and scaling-up the micro-reactors for gram-scale synthesis has proven to be challenging.[25,28–30] In addition, microfluidic reactors are time-consuming to fabricate and expensive, and reactor fouling during synthesis can results in long delays.[28,30,31]

Most automated systems are developed with the user in mind, meaning that the inclusion of open-source electronics platforms such as an Arduino or Raspberry Pi promotes easy access, configuration, and operation without the need for expertise in hardware or software design. The major goal is to enable the seamless integration of such technologies into a lab workflow to aid continual project development while maintaining exceptional quality control. In this paper, we detail the design and application of a low-cost, portable, semi-automated instrument using a Raspberry Pi and 3D printed† parts that is capable of reproducibly synthesizing GNPs *via* the Turkevich method.

Materials and methods

Gold nanoparticle (AuNP) synthesis

AuNPs were produced using a citrate reduction method, following an adapted Turkevich protocol. For a standard synthesis, auric acid was prepared by dissolving Gold(III) chloride trihydrate (Millipore Sigma, 99.995% purity) to achieve a concentration of 1 mM in a volume of 12.5 mL, which was then introduced into a 250 mL Erlenmeyer flask. Water was added to reach a final solution volume of 100 mL. The gold solution

was heated to 100 °C, while being stirred at a rate of 250 rpm with a 20 mm Teflon-coated magnetic stir bar. This setup, including the choice of flask, stirring speed, and stir bar size, was strategically chosen to enhance the mixing efficiency of the reaction and to prevent the solution from splashing along the flask's interior during the nanoparticle synthesis. The gold solution was heated for 7 min, which was calculated to be the optimum time taken to reach the boiling point. Once boiling, trisodium citrate (3–10 mL, 0.1% w/v) was added to the gold solution and the reaction was left to proceed for 15 min. According to the Turkevich method, the diameters of gold nanospheres can be controlled by varying the volume of citrate used in the AuNP synthesis procedure. Therefore, we explored the effect that changing citrate volumes across a range of 3–10 mL would have on the diameters. The volume of water and gold solution were fixed at 87.5 mL and 12.5 mL, respectively.

Characterization of the gold nanospheres

UV-Vis spectra were collected using a Tecan Infinite 200 Pro across a range of 350–800 nm at 1 nm resolution. To aid spectral comparisons each spectrum was normalized using the absorbance value of the lambda max (λ_{max}). Images of the nanospheres were acquired using a 100 kV JEOL 1200 EX transmission electron microscope (TEM). All images were collected at 150 K magnification. Image J software was used to measure the size of the AuNPs. As AuNPs above 40 nm that are synthesized using the Turkevich method tend to start to develop a more oval shape, measurements were taken across the smallest AuNP width to overcome issues associated with larger particles synthesized using smaller volumes of citrate becoming more oval.

### NanoSynth mini construction

The NanoSynth Mini consists of three different assembled parts; a controller, a pump(s) and a dispensing arm. The system also makes use of general laboratory equipment such as an external stirrer hotplate, lab jack, and support rod which are controlled and adjusted manually by the instrument operator. The three parts of the Nanosynth Mini are comprised of readily available components which are either housed-in or attached to 3D printed accessories. Fig. 1 shows a photograph of the instrument alongside the assembled parts and components.

Raspberry Pi, motor driver hardware attached on top (HAT) and electronic components

Two 20 female stacking header pins were soldered to the underside of the motor driver HAT (Adafruit, US) to allow direct attachment to the general-purpose input/output (GPIO) pins of the Raspberry Pi board. The HAT can support a maximum of 4 DC motors using an external 12 V power supply capable of delivering 1.2A to each motor with a peak power of 3A. To power the motors we used a female Jack plug adapter connector (2.1 × 5.5 mm), which allows a standard 12 V 5A DC power supply to be connected. To enable the pumping of

---

† 3D print files and Python code developed as part of this project will be made available upon request.
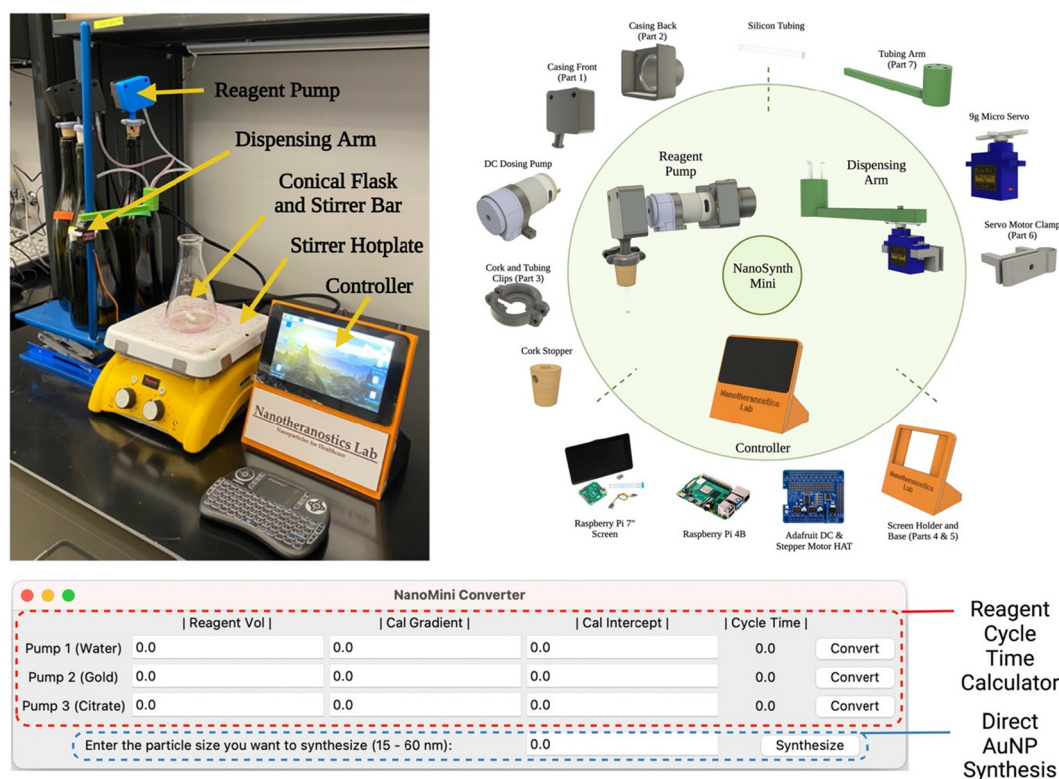
Fig. 1 The NanoSynth Mini instrument, assembled parts, components, and an operational GUI. The photograph shows the NanoSynth Mini setup, including the dispensing arm, reagent pump, and controller assembled parts, and general laboratory equipment including a stirrer hotplate, a conical flask containing a magnetic stirring bar, and a lab jack with a support rod attached. Also shown are each of the assembled parts and their components with 3D-printed attachments or housings. The NanoMini Converter GUI is optimized to calculate the reagent pump cycle time depending on reagent volume and gradient and intercept taken from pump calibration curves. The GUI is also capable of automatically synthesizing AuNPs with user-specified sizes according to the citrate reduction protocol.

reagents we acquired three Gikfun AE1207 12 V DC dosing pumps. Terminal block connectors were used to attach the motors to the HAT. A tutorial outlining the preparation of the HAT is given on the Adafruit website (**https://learn.adafruit.com/adafruit-dc-and-stepper-motor-hat-for-raspberry-pi/assembly**). For the peripheral HAT to communicate with the Pi it is necessary to initiate I2C communication in the kernel. After enabling the I2C and verifying that the Pi is running Python 3, CircuitPython Motorkit software is installed on the Raspberry Pi.

Controller screen and nanoparticle size selection GUI

The Raspberry Pi and Motor Driver HAT were attached to the underside of a Raspberry PI 7″ touchscreen using M2.5 brass hex spacers and then housed in a 3D printed screen holder and base (parts 4&5, Fig. 1) which are adhered together. The Pi is then connected to the screen *via* a ribbon cable attached to the display port and two jumper cables connected to the 5 V and ground pins. A mini Bluetooth keyboard was connected to the Pi to provide cursor control and text input for interfacing with the microprocessor. The GUI (NanoMini Converter) for operating the NanoSynth Mini is shown in Fig. 1. The interface contains a region for inputting the pump calibration curve

parameters including gradient and intercept to calculate the cycle time required to dispense a specific amount of reagent. It also features a section whereby the user can enter their desired AuNP size from 15–60 nm and the instrument will automatically synthesize a batch of nanoparticles according to a citrate reduction protocol. For nanoparticles of accurate size to be produced the user also needs to input the calibration curve parameters but can leave the reagent volume input blank.

Dosing pump enclosure and calibration

The 3D-printed enclosures for the dosing pumps are designed to enable portability and to allow the pumps to be inserted directly into a standard wine bottle used to store the reagents. Three enclosure components were designed on Fusion 360: a front case (part 1, Fig. 1), a back case (part 2, Fig. 1), and cork and tubing clips (part 3, Fig. 1). The parts were fabricated using an Elegoo Mars 2 Pro resin printer from grey UV-curing standard photopolymer resin. Fig. 1 shows the reagent pump and enclosure configuration. Silicon tubing was attached to each end of the pump and threaded through the holes on the underside of the front plate. The DC pump was then screwed to the front plate. The back plate was inserted over the motor and screwed to the front plate to form the full enclosure. A

cork is used to plug the wine bottles and support the pump. The cork (15/16″ × 47/64″) features an 8 mm hole drilled vertically through the center and a 6 mm hole penetrating the side approximately 4 mm from the top of the cork. The 6 mm hole penetrates the center hole, to enable airflow. Silicon tubing attached to the drawing side of the DC motor is threaded through the vertical hole in the cork. The cork is then secured to the motor enclosure using the cork locking hinge. The silicon tubing attached to the dispensing side of the pump is threaded through the dispensing arm. Adjusting the dosage pump rotation time allows different volumes of reactants to be delivered to the reaction flask. Calibration curves for each pump were generated using distilled water because all the synthesis reagents were aqueous. The water and the reagents used to synthesize the AuNPs were stored in wine bottles which were chosen based on their ability to prevent oxidation and limit light exposure. The water was pumped from the wine bottles to a volumetric flask which was weighed after each cycle. Two different ranges of dispensing times 10–100 s (10 s intervals, 3 reps of each interval) and 3–9 s (1 s intervals, 3 reps of each interval) which accommodate all reactant dispensing volumes explored in the synthesis of GNPs.

Dispensing arm design and control

The servo-operated dispensing arm (Fig. 1) is composed of a 3D printed servo motor clamp (part 6, Fig. 1) for attachment of the dispensing arm to the support rod, a 3D printed tubing arm to support the silicon tubing for reagent dispensing (part 7, Fig. 1), and a 9 g micro servo motor for controlling arm movement. The dispensing arm can be controlled across a rotation of 90°. At 0° (neutral position) the arm is positioned at the side of the reagent vessels away from the hotplate, while at 90° (delivery position) the arm is suspended above the reaction vessel for reagent transfer. Once all the reagent is dispensed the arm returns to its neutral position. Arm movement means that heat generated by the hotplate does not cause the tubing arm to bend leading to inaccurate reagent transfer.

Results

Reagent pump calibration

The calibration curves for the three reagent pumps are shown in Fig. 2, plots for the 10–100 s range are shown on the top row and 3–9 s on the bottom row. Each curve shows excellent linearity ($R^2 \geq 0.9999$) with very limited variation observed between replicate measurements. The linear equations were then used to calculate how much time is required (s) to dispense a specific volume of reagent (e.g., to dispense 100 mL of aqueous reagent using pump 1 would take 85.4 s). For reaction purposes, pump 1 was assigned to dispense water, pump 2 dispensed the gold solution, and pump 3 was used to dispense the trisodium citrate solution. To ensure uniformity in our procedures, we periodically dispensed and assessed individual water volumes, confirming their alignment with the expectations set by the calibration curve.

UV-Vis analysis of spherical AuNPs

Three replicate batches of gold nanospheres were synthesized using 3, 4, 5, 7.5, 8.5, and 10 mL of trisodium citrate solution. The stacked plots in Fig. 3 show the normalized absorbance spectra measured for three replicate batches of nanoparticles across the citrate volume range (3–10 mL). Also shown in Fig. 3
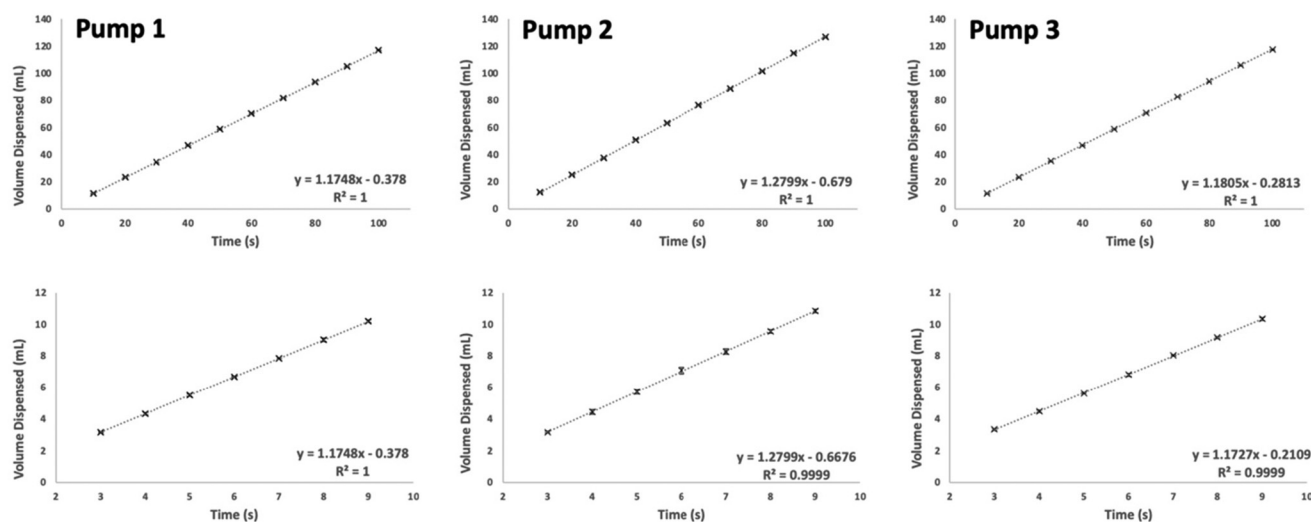
Fig. 2 Calibration curves were generated for the three reagent dispensing pumps. The reagent pumps were configured to deliver water contained within the wine bottles to the reaction vessel for two set time periods (10–100 s, displayed on the top row) and (3–9 s, displayed on the bottom row). After each transfer, the reaction vessel was weighed to ascertain the volume of water dispensed. Three replicates were measured at each cycle time. Each pump exhibits an excellent linear relationship between cycle time and volume dispensed. The standard variations are included on the curves but are barely visible due to the accuracy of the pumps. The gradient and intercept shown on the plots are inputted into the GUI to enable cycle time calculation and automated AuNP synthesis.
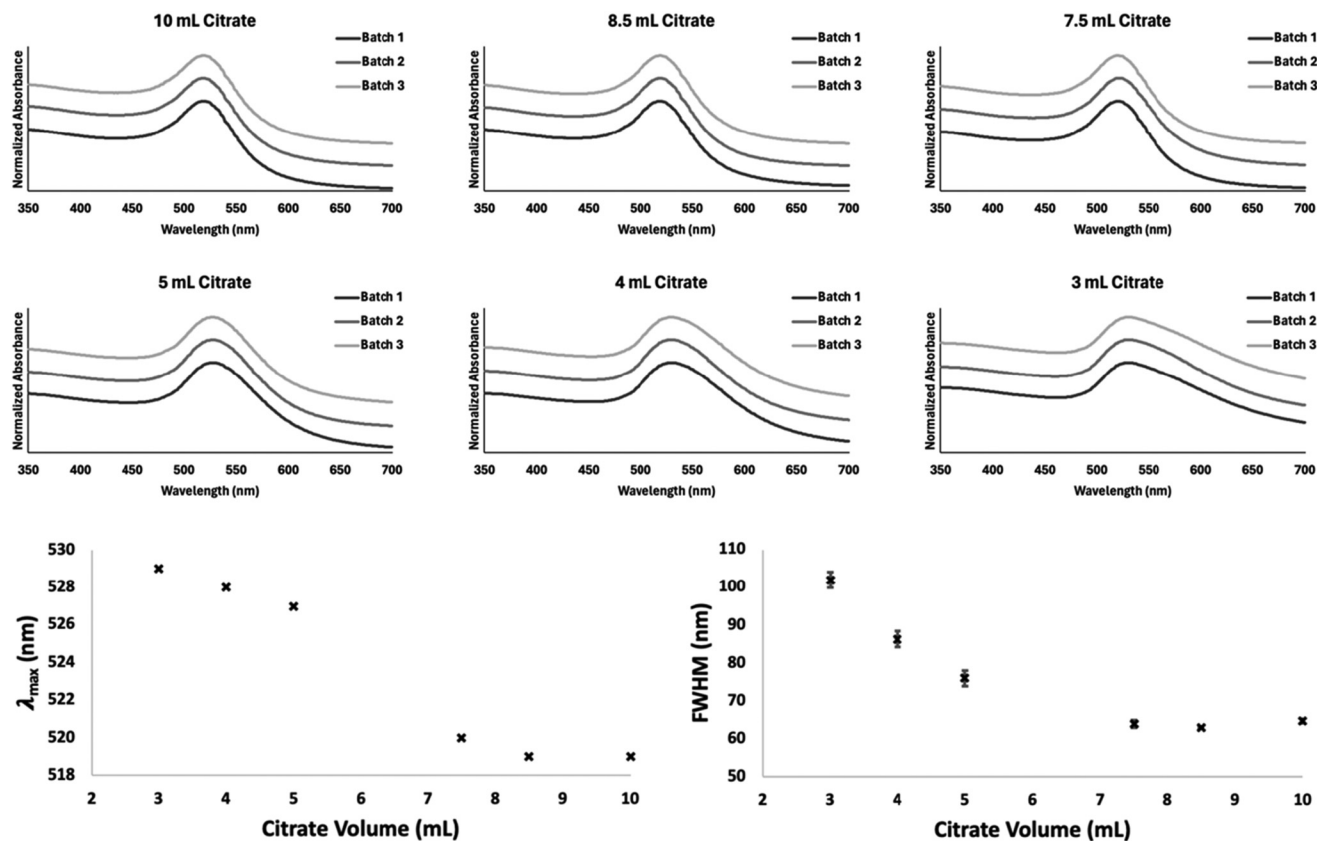
Fig. 3 Replicate (n = 3) normalized UV-Vis spectra of AuNPs synthesized using different volumes of citrate solution (0.1% w/v) and plots showing the relationship between citrate volume, $\lambda_{\max}$, and full-width-half-maximum. Stacked Offset plots show the normalized UV-Vis spectra collected from three repeat batches of AuNPs synthesized using 10 mL, 8.5 mL, 7.5 mL, 5 mL, 4 mL, and 3 mL of citrate solution. Below shows the sigmoidal relationship between citrate volume and $\lambda_{\max}$. The standard deviation in measured $\lambda_{\max}$ for the replicate syntheses is 0. The relationship between citrate volume and full-width-half-maximum (FWHM) demonstrated that excellent batch-to-batch FWHM reproducibility is obtained (≤2.08 nm).

are plots displaying the relationship between citrate volume, measured $\lambda_{\max}$, and full-width-half-maximum (FWHM). Each replicate batch of AuNPs generated using the same volume of citrate display excellent UV-Vis spectral reproducibility, this is also evidenced by the lack of variation in $\lambda_{\max}$ between replicates.

The sigmoidal relationship between citrate volume and observed $\lambda_{\max}$ values align with previously published research that greater concentrations of citrate cause the $\lambda_{\max}$ to shift towards lower wavelengths. When less than 3 mL of citrate was used to reduce the gold solution the AuNPs became unstable and agglomerated immediately post-synthesis. This is most likely due to there not being enough citrate molecules surrounding the gold nanospheres to induce coulombic repulsion. When citrate volumes >10 mL were used, we observed no further decrease in nanosphere diameters. This means that the Turkevich reaction is only capable of proceeding whilst the molar ratio of citrate : Au is within a 1.27–4.23 range. As can be seen in Fig. 3 minimal batch-to-batch variation in the FWHM (≤2.08 nm) is observed between replicate synthesizes at each citrate volume.

TEM analysis of spherical AuNPs

Example TEM images corresponding to AuNPs synthesized using different volumes of citrate are shown in Fig. 4A. The table in Fig. 4B shows the average AuNP diameters calculated for each replicate batch, the average AuNP diameters calculated across batches, and the standard deviation associated with the AuNP diameters. It can be observed in both the TEM images and the summary table that as the volume of citrate increases the AuNP size decreases. Batch-to-batch variation in AuNP size varies from 0.3 nm (10 mL citrate; AuNPs = 15.5 nm diameter) to 4.4 nm (3 mL citrate; AuNPs = 60.7 nm). In general, the standard deviation associated with the average AuNP diameter calculated across all batches increases as the particles get bigger; 47.3 nm AuNPs synthesized using 4 mL of citrate is the only outlier in this trend. The nonlinear relationship between citrate volume and the size of GNPs across a range of 15–60 nm can be described using a 2nd order polynomial (R^2 = 0.9968) shown in Fig. 4C. Once we had derived the mathematical relationship between citrate volume and nanoparticle size it was possible to utilize the equation of the
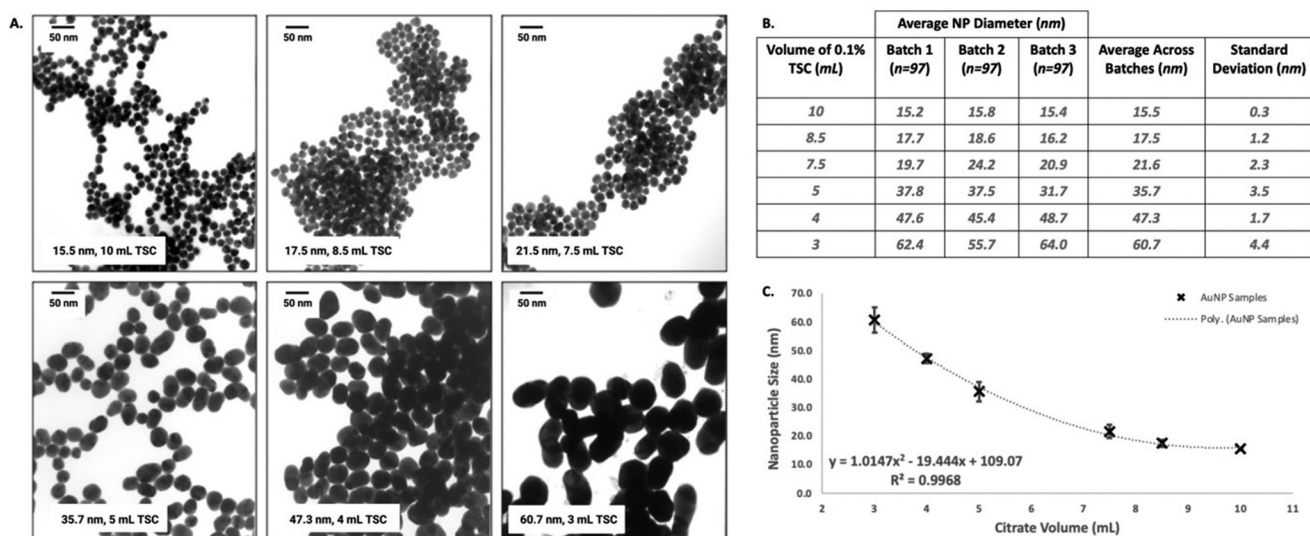
Fig. 4 TEM Analysis. (A) Shows TEM images of the AuNPs synthesized using different volumes of citrate solution. The average measured size of the AuNPs calculated across three replicate syntheses is inset in each image along with the volume of citrate used. (B) The table shows the average AuNP diameter estimated for each batch of AuNPs (n = 97 particles measured), the average AuNP diameter calculated across all batches, and their standard deviation (nm). (C) Describes the polynomial relationship between AuNP size and the citrate volume (R^2 = 0.9968), the 2nd order polynomial equation used to define the relationship is displayed.

trendline displayed in Fig. 4C to develop the GUI shown in Fig. 1 that could automatically calculate the right amount of citrate required according to the user's AuNP size requirements. Using coefficients, a = 1.0147, b = −19.444, constant c = 109.07 (derived from the trendline), and y = required AuNP size (*e.g.*, 20 nm) the real component associated with the downward trend in the parabola can be calculated using the quadratic equation solving for x (*e.g.*, synthesis of 20 nm AuNPs would require 7.58 mL of citrate solution). Once the amount of citrate has been calculated it is then possible to calculate pump dispensing time using the linear equations from the dosage pump calibration curves. The equation for pump 3, used to dispense citrate solution is y = 1.173x–0.2129 (Fig. 3) so solving for x using y which corresponds to citrate volume (mL) reveals the dispensing time. Therefore, to produce 20 nm AuNPs would require 7.58 mL of citrate solution which is dispensed by pump 3 in 6.64 s. The open-source python-based GUI titled 'NanoMini Converter' shown in Fig. 1 has been developed to automate the calculations above. The converter can either be coupled to the NanoSynth Mini or used as a standalone GUI to aid manual spherical AuNP synthesis *via* citrate reduction.

Testing the accuracy of NanoSynth mini

Six test batches of AuNPs were synthesized using the NanoSynth Mini interfaced with the NanoMini Converter to test the accuracy of the system to produce AuNPs of a specific size. Citrate volumes of 3.5, 4.5, 5.5, 6.5, 8, and 9 mL were tested. Based on our understanding of the relationship between nanoparticle size and citrate volume we calculated the expected size of the nanoparticles to be 53.4 nm (3.5 mL), 42.1 nm (4.5 mL), 32.8 nm (5.5 mL), 25.6 nm (6.5 mL), 18.5 nm (8 mL), and 16.3 nm (9 mL). The TEM images repre-
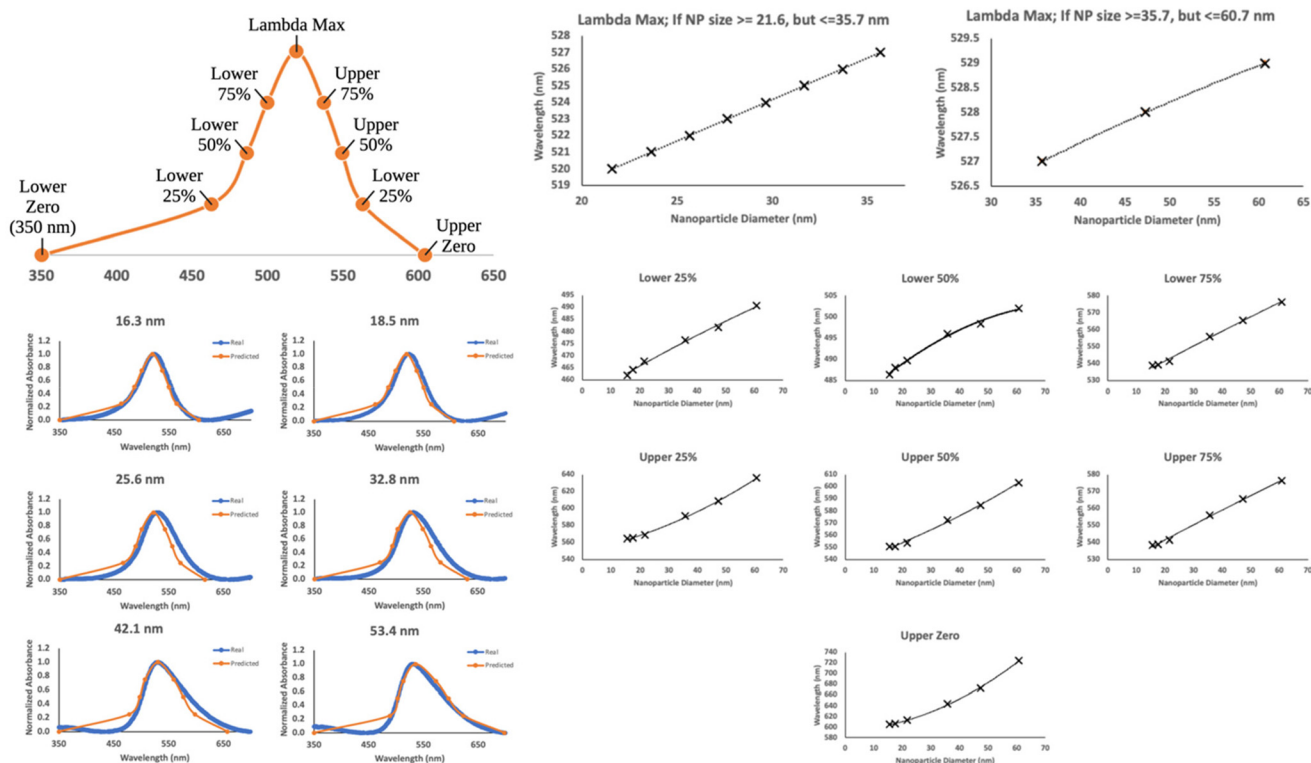
sentative of the six test batches is shown in Fig. 5A. As expected, visual analysis of the images indicates that as citrate volume increases AuNP size decreases. The average AuNP size was estimated for each test batch based on measurements taken from ~100 NPs using ImageJ software. The average values (represented as black diamonds) were plotted on top of the curve shown in Fig. 4B to generate Fig. 5B. Excellent agreement between the model and test data is observed in Fig. 5B, meaning that the NanoSynth Mini can automate the citrate reduction-based spherical AuNP synthesis process according to user-defined size requirements. The table in Fig. 5C summarizes the results between the expected and actual AuNP size. The average difference between the expected and actual AuNPs size was calculated to be 1.21 ± 0.78 nm which further demonstrates the instrument's ability to accurately produce AuNPs according to a defined size.

Using our previously generated UV-Vis data as a model we then decided to evaluate its ability to predict the UV-Vis spectra of the AuNPs synthesized in our test batches. All UV-Vis data was truncated to a 350–750 nm spectral range, baseline corrected using an asymmetric least squares algorithm, and then normalized to 1 using the absorbance at the λ_{max}. The wavelength values at 9 different sites on the model UV-Vis data (shown in Fig. 6) were then correlated to AuNP diameter. The lower zero was set at 350 nm and the λ_{max} of AuNPs <21.6 nm in diameter was set at 519 nm in accordance with our previous observations. To establish the λ_{max} for nanoparticles falling within the ≥21.6–≤35.7 nm range linear regression was used to predict the values according to the λ_{max} measured for the 21.6 and 35.7 nm AuNPs. A linear equation (y = 0.0799x + 524.17) based on the λ_{max} measured for 35.7, 47.3, and 60.7 nm was used to predict the λ_{max} of nano-
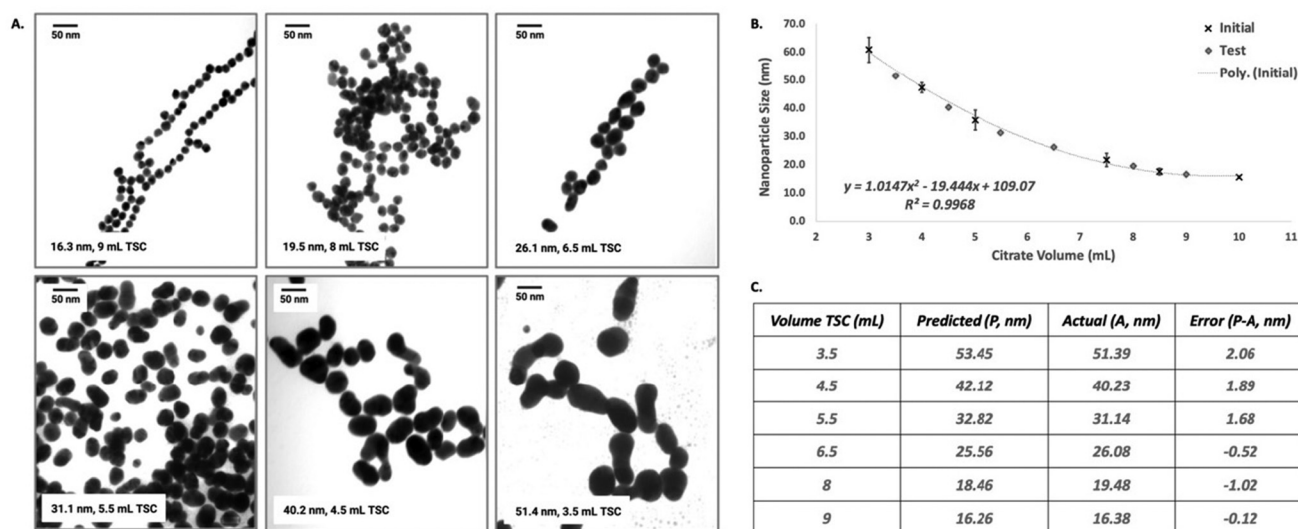
Fig. 5 Evaluation of Test AuNP batches. (A) Shows TEM images of the Test batches of AuNPs synthesized using 9 mL, 8 mL, 6.5 mL, 5.5 mL, 4.5 mL, and 3.5 mL of citrate solution. The average size of the AuNPs inset in each image along with the volume of citrate used. (B) The red diamonds representative of the test batch AuNP sizes is overlayed onto the plot previously shown in (C). (C) The table displays the predicted size of the test AuNPs based on the amount of citrate used (p) and the actual size calculated from the TEM images (A). The error between prediction and actual (P−A) for the test batches is shown in the final column. The average error between P and A across all test batches was calculated to be 1.21 ± 0.78 nm.

$$y = 1.0147x^2 - 19.444x + 109.07$$
$$R^2 = 0.9968$$

Volume TSC (mL)	Predicted (P, nm)	Actual (A, nm)	Error (P-A, nm)
3.5	53.45	51.39	2.06
4.5	42.12	40.23	1.89
5.5	32.82	31.14	1.68
6.5	25.56	26.08	-0.52
8	18.46	19.48	-1.02
9	16.26	16.38	-0.12

Fig. 6 The UV-Vis data collected from the nanoparticles synthesized using 3, 4, 5, 7.5, 8.5, and 10 mL of trisodium citrate was used as a model to prediction the UV-Vis spectra collected from the batch of test AuNPs synthesized using 3.5, 4.5, 5.5, 6.5, 8, and 9 mL of trisodium citrate. The absorbance values of 9 separate datapoints were measured in each of the model UV-Vis data which had been baseline corrected and normalized. Overlays of the predicted and actual UV-Vis spectra collected from the test samples show excellent agreement. The plots on the right display the observed trends for each data point as a function of nanoparticle diameter.

particles between $>35.7-\leq60.7$ nm in size. The relationship between the wavelength of the model data at the upper zero point and AuNP size is well described using 2nd order polynomial trendline ($y = 0.033x^2 + 0.1517x + 592.98$, $R^2 = 0.9986$). Three lower and upper wavelength values were measured from each side of the peak maximum corresponding to 25%, 50%, and 75% of total absorbance. Their wavelengths were calculated relative to the λ_{max} so that the morphology of the peak was better understood. The relationship between the lower and upper values for each percentage absorbance along with the equations for the curves is shown in Fig. 6. The relationships established between the extracted wavelength values from the model UV-Vis data and AuNP size were then used to generate UV-Vis spectral predictions for the test data (Fig. 6). There is a significant overlap observed between the predicted spectra and the real spectra observed for all the test batches. Remarkably, the model values are also capable of predicting the broadening of the UV-Vis peak displayed most prominently by 42.1 and 53.4 nm AuNPs. While there doesn't appear to be a significant difference between the predicted and real spectra for 25.6 and 32.8 nm AuNPs there is a slight wavelength difference between the two peaks which occurs after the peak maxima. This is possibly due to the use of linear regression to predict the λ_{max} values for AuNPs that fall within the $\geq21.6-\leq35.7$ nm size range as all upper wavelength values apart from the zero value were calculated relative to the estimated λ_{max}.

Conclusion and discussion

The NanoSynth Mini is a proficient automated system for producing spherical AunPs *via* citrate-reduction. Its integration of a Raspberry Pi microcontroller assures a consistent output of gold AuNPs with remarkable batch-to-batch consistency. With its capacity for precise citrate dispensing, the system enables exact adjustments to the nanoparticle diameter, thereby standardizing the quality of nanoparticle solutions. The incorporation of UV-Vis spectroscopy data into predictive models directly correlates citrate concentration with particle size, further refining the synthesis process. While the time required for automated synthesis is comparable to manual methods, and both are expected to yield nanoparticles with similar long-term stability due to the identical underlying protocol, the NanoSynth Mini distinguishes itself by facilitating a more controlled and error-free experimental process. This precision greatly benefits the uniformity of the nanoparticles, which is crucial for the performance of downstream applications, from diagnostic biosensors to electronic and photonic devices that depend on exact nanoparticle specifications. Moreover, the affordability and open-source design of the NanoSynth Mini, coupled with its compatibility with standard laboratory equipment, render it an advantageous addition to research settings. By improving batch-to-batch reliability, the NanoSynth Mini presents not just an improvement in efficiency but a potential shift in the laboratory approach to nanoparticle synthesis.

The automation provided by the NanoSynth Mini is anticipated to evolve, expanding its functionality to include more dispensing pumps and sophisticated Python scripts for managing more complex synthesis procedures. These developments are expected to unlock the ability to automate the production of nanoparticles with intricate shapes and to increase the scale of production.

Author contributions

Suhash Reddy Chavva: investigation, methodology, writing original draft. Angela Michelle T. San Juan: investigation, characterization. Siddhant Jaitpal: investigation, characterization. Ngoc Nhu Vu: characterization. Samuel Mabbott: project administration.

Conflicts of interest

The authors have a provisional patent filed for the technology described within this manuscript.

Acknowledgements

References

1 D. T. Thompson, Using Gold Nanoparticles for Catalysis, *Nano Today*, 2007, **2**(4), 40–43, DOI: **10.1016/S1748-0132(07)70116-0**.

2 S. A. C. Carabineiro, Supported Gold Nanoparticles as Catalysts for the Oxidation of Alcohols and Alkanes, *Front. Chem.*, 2019, 7, DOI: **10.3389/fchem.2019.00702**.

3 T. Ishida, A. Taketoshi and M. Haruta, Gold Nanoparticles for Oxidation Reactions: Critical Role of Supports and Au Particle Size, in *Topics in Organometallic Chemistry*, 2020.

4 L. A. Dykman and N. G. Khlebtsov, Gold Nanoparticles in Chemo-, Immuno-, and Combined Therapy: Review [Invited], *Biomed. Opt. Express*, 2019, **10**(7), 3152–3182, DOI: **10.1364/boe.10.003152**.

5 S. Jain, D. G. Hirst and J. M. O'Sullivan, Gold Nanoparticles as Novel Agents for Cancer Therapy, *Br. J. Radiol.*, 2012, **85**(1010), 101–113.

6 X. Gu, Z. Xu, L. Gu, H. Xu, F. Han, B. Chen and X. Pan, Preparation and Antibacterial Properties of Gold Nanoparticles: A Review, *Environ. Chem. Lett.*, 2020, **19**, DOI: **10.1007/s10311-020-01071-0**.

7   S. Shamaila, N. Zafar, S. Riaz, R. Sharif, J. Nazir and S. Naseem, Gold Nanoparticles: An Efficient Antimicrobial Agent against Enteric Bacterial Human Pathogen, *Nanomaterials (Basel)*, 2016, **6**(4), 71, DOI: 10.3390/nano6040071.

8   X. Li, S. M. Robinson, A. Gupta, K. Saha, Z. Jiang, D. F. Moyano, A. Sahar, M. A. Riley and V. M. Rotello, Functional Gold Nanoparticles as Potent Antimicrobial Agents against Multi-Drug-Resistant Bacteria, *ACS Nano*, 2014, **8**(10), 10682–10686, DOI: 10.1021/nn5042625.

9   G. Zhang, Functional Gold Nanoparticles for Sensing Applications, *Nanotechnol. Rev.*, 2013, **2**(3), 269–288, DOI: 10.1515/ntrev-2012-0088.

10 C. C. Chang, C. P. Chen, T. H. Wu, C. H. Yang, C. W. Lin and C. Y. Chen, Gold Nanoparticle-Based Colorimetric Strategies for Chemical and Biological Sensing Applications, *Nanomaterials (Basel)*, 2019, **9**(6), 861.

11 K. Saha, S. S. Agasti, C. Kim, X. Li and V. M. Rotello, Gold Nanoparticles in Chemical and Biological Sensing, *Chem. Rev.*, 2012, **112**(5), 2739–2779.

12 F. Mafuné, J. Y. Kohno, Y. Takeda, T. Kondow and H. Sawabe, Formation of Gold Nanoparticles by Laser Ablation in Aqueous Solution of Surfactant, *J. Phys. Chem. B*, 2001, **105**(22), 5114–5120, DOI: 10.1021/jp0037091.

13 D. Yang, S. Lee, B. Chen and S. Nikumb, Fabrication of Gold Nanoparticles by Pulsed Laser Ablation in Aqueous Media, *J. Laser Micro/Nanoeng.*, 2008, **3**(3), 147–151, DOI: 10.2961/jlmn.2008.03.0004.

14 B. J. Y. Tan, C. H. Sow, T. S. Koh, K. C. Chin, A. T. S. Wee and C. K. Ong, Fabrication of Size-Tunable Gold Nanoparticles Array with Nanosphere Lithography, Reactive Ion Etching, and Thermal Annealing, *J. Phys. Chem. B*, 2005, **109**(22), 11100–11109, DOI: 10.1021/jp045172n.

15 J. Turkevich, P. C. Stevenson and J. Hillier, A Study of the Nucleation and Growth Processes in the Synthesis of Colloidal Gold, *Discuss. Faraday Soc.*, 1951, **11**, 55–75, DOI: 10.1039/DF9511100055.

16 G. Frens, Controlled Nucleation for the Regulation of the Particle Size in Monodisperse Gold Suspensions, *Nat. Phys. Sci.*, 1973, **241**, 20–22, DOI: 10.1038/physci241020a0.

17 D. R. Baer, The Chameleon Effect: Characterization Challenges Due to the Variability of Nanoparticles and Their Surfaces, *Front. Chem.*, 2018, **6**, DOI: 10.3389/fchem.2018.00145.

18 M. Thiele, J. Z. E. Soh, A. Knauer, D. Malsch, O. Stranik, R. Müller, A. Csáki, T. Henkel, J. M. Köhler and W. Fritzsche, Gold Nanocubes - Direct Comparison of Synthesis Approaches Reveals the Need for a Microfluidic Synthesis Setup for a High Reproducibility, *Chem. Eng. J.*, 2016, **288**, 432–440, DOI: 10.1016/j.cej.2015.12.020.

19 N. Hartrampf, A. Saebi, M. Poskus, Z. P. Gates, A. J. Callahan, A. E. Cowfer, S. Hanna, S. Antilla, C. K. Schissel, A. J. Quartararo, *et al.* Synthesis of Proteins by Automated Flow Chemistry, *Science*, 2020, **368**(6494), 980–987, DOI: 10.1126/science.abb2491.

20 M. Panza, S. G. Pistorio, K. J. Stine and A. V. Demchenko, Automated Chemical Oligosaccharide Synthesis: Novel Approach to Traditional Challenges, *Chem. Rev.*, 2018, **118**(17), 8105–8150.

21 N. Collins, D. Stout, J. P. Lim, J. P. Malerich, J. D. White, P. B. Madrid, M. Latendresse, D. Krieger, J. Szeto, V. A. Vu, *et al.* Fully Automated Chemical Synthesis: Toward the Universal Synthesizer, *Org. Process Res. Dev.*, 2020, **24**(10), 2064–2077, DOI: 10.1021/acs.oprd.0c00143.

22 D. Salley, G. Keenan, J. Grizou, A. Sharma, S. Martín and L. Cronin, A Nanomaterials Discovery Robot for the Darwinian Evolution of Shape Programmable Gold Nanoparticles, *Nat. Commun.*, 2020, **11**, 2771, DOI: 10.1038/s41467-020-16501-4.

23 H. Huang, H. Du Toit, S. Ben-Jaber, G. Wu, L. Panariello, N. T. K. Thanh, I. P. Parkin and A. Gavriilidis, Rapid Synthesis of Gold Nanoparticles with Carbon Monoxide in a Microfluidic Segmented Flow System, *React. Chem. Eng.*, 2019, **4**, 884–890, DOI: 10.1039/c8re00351c.

24 S. E. Lohse, J. R. Eller, S. T. Sivapalan, M. R. Plews and C. J. Murphy, A Simple Millifluidic Benchtop Reactor System for the High-Throughput Synthesis and Functionalization of Gold Nanoparticles with Different Sizes and Shapes, *ACS Nano*, 2013, **7**(5), 4135–4150, DOI: 10.1021/nn4005022.

25 J. Wagner, T. R. Tshikhudo and J. M. Köhler, Microfluidic Generation of Metal Nanoparticles by Borohydride Reduction, *Chem. Eng. J.*, 2008, **135**(1), S104–S109, DOI: 10.1016/j.cej.2007.07.046.

26 H. Du Toit, T. J. Macdonald, H. Huang, I. P. Parkin and A. Gavriilidis, Continuous Flow Synthesis of Citrate Capped Gold Nanoparticles Using UV Induced Nucleation, *RSC Adv.*, 2017, **7**, 9632–9638, DOI: 10.1039/c6ra27173a.

27 V. S. Cabeza, S. Kuhn, A. A. Kulkarni and K. F. Jensen, Size-Controlled Flow Synthesis of Gold Nanoparticles Using a Segmented Flow Microfluidic Platform, *Langmuir*, 2012, **28**(17), 7007–7013, DOI: 10.1021/la205131e.

28 Y. Song, J. Hormes and C. S. S. R. Kumar, Microfluidic Synthesis of Nanomaterials, *Small*, 2008, **4**(6), 698–711, DOI: 10.1002/smll.200701029.

29 C. J. Richmond, H. N. Miras, A. R. De La Oliva, H. Zang, V. Sans, L. Paramonov, C. Makatsoris, R. Inglis, E. K. Brechin, D. L. Long, *et al*. A Flow-System Array for the Discovery and Scale up of Inorganic Clusters, *Nat. Chem.*, 2012, **4**(12), 1037–1043, DOI: 10.1038/nchem.1489.

30 S. Biswas, J. T. Miller, Y. Li, K. Nandakumar and C. S. S. R. Kumar, Developing a Millifluidic Platform for the Synthesis of Ultrasmall Nanoclusters: Ultrasmall Copper Nanoclusters as a Case Study, *Small*, 2012, **8**(5), 688–698, DOI: 10.1002/smll.201102100.

31 Y. Li, A. Sanampudi, V. Raji Reddy, S. Biswas, K. Nandakumar, D. Yemane, J. Goettert and C. S. S. R. Kumar, Size Evolution of Gold Nanoparticles in a Millifluidic Reactor, *ChemPhysChem*, 2012, **13**, 177–182, DOI: 10.1002/cphc.201100726.